NANO LETTERS

2006
Vol. 6, No. 7
1535−1540

Composite-Hydroxide-Mediated Approach for the Synthesis of Nanostructures of Complex Functional-Oxides

Hong Liu,[†,‡] Chenguo Hu,[†,§] and Zhong Lin Wang*,[†,||,⊥]

School of Materials Science and Engineering, Georgia Institute of Technology, Atlanta, Georgia 30332-0245, State Key Laboratory of Crystal Materials, Shandong University, Jinan 250100 P R China, Department of Applied Physics, Chongqing University, Chongqing 400044, China, College of Engineering, Peking University, Beijing, China, and National Center for Nanoscience and Technology of China, Beijing, 100080, China

Received June 1, 2006

ABSTRACT

We demonstrate a generic approach for the synthesis of single-crystal complex oxide nanostructures of various structure types, such as perovskites, spinels, monoclinic, corundum, CaF_2 structured, tetragonal, and even metal hydroxides. The method is based on a reaction between a metallic salt and a metallic oxide in a solution of composite-hydroxide eutectic at ~200 °C and normal atmosphere without using an organic dispersant or capping agent. The synthesis technique is cost-effective, one-step, easy to control, and is performed at low temperature and normal atomospheric pressure. The technique can be expanded to many material systems, and it provides a general, simple, convenient, and innovative strategy for the synthesis of nanostructures of complex oxides with important scientific and technological applications in ferroelectricity, ferromagnetism, colossal magnetoresistance, fuel cell, optics, and more.

Complex oxides with structures such as perovskite, spinel, and garnet have many important properties and applications in science and engineering, such as ferroelectricity, ferromagnetism, colossal magnetoresistance, semiconductors, luminance, and optoelectronics.[1−6] Nanostructures (nanoparticles, nanowires, and nanobelts) of complex oxides have attracted much attention because of their size-induced novel properties. Although some synthesis methods are successful for fabricating single-cation oxide nanocrystals,[7−14] only a limited amount of work is available for synthesizing nanostructures of complex oxides (with two or more types of cations) because of difficulties in controlling the composition, stoichiometry, and/or crystal structure. The existing techniques rely on high pressure, salt-solvent-mediated high temperature, surface-capping agent, or organometallic precursor-mediated growth process,[15−24] and the types of oxides that can be synthesized are rather limited. Therefore, seeking a simple approach for low-cost, lower-temperature, large-scale, controlled growth of oxide nanostructures at atmospheric pressure is highly desired, and it is important for exploring zero- and one-dimensional complex oxide-based nanostructures for applications in nanodevices and nanosystems.

Here we report a general and widely applicable approach for the synthesis of complex oxide nanostructures of scientific and technological importance. The method is based on a reaction between a metallic salt and a metallic oxide in a solution of molten mixed potassium hydroxide and sodium hydroxide eutectic at ~200 °C and normal atmosphere without using an organic dispersant or capping agent. This methodology provides a one-step, convenient, low-cost, nontoxic, and mass-production route for the synthesis of nanostructures of functional oxide materials of various structure types.

We now use the synthesis of two families of complex oxides, perovskite (ABO_3; $A_xA'_{1-x}BO_3$; $AB_xB'_{1-x}O_3$)[25] and spinel (AB_2O_4), to illustrate the principle and applications of the approach. The sources of A and A′ cations are from metallic salts, such as nitrates, chlorates, or acetates, and the sources for B and B′ cations are from oxides with valence states that match those present in the desired product to be synthesized. The mixed hydroxides are used to not only mediate the reactions between the raw materials containing

* To whom correspondence should be addressed. E-mail: zhong.wang@mse.gatech.edu.
[†] Georgia Institute of Technology.
[‡] Shandong University.
[§] Chongqing University.
[||] Peking University.
[⊥] National Center for Nanoscience and Technology of China.

10.1021/nl061253e CCC: $33.50
Published on Web 06/27/2006

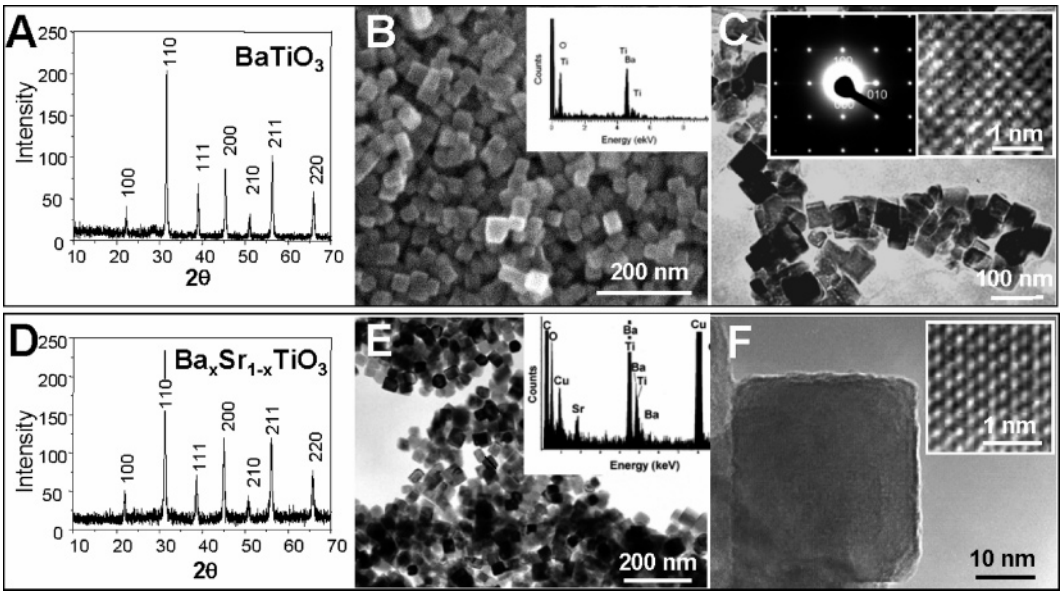

Figure 1. Synthesis of perovskite nanostructures. (A−C) $BaTiO_3$ and (D−F) $Ba_xSr_{1-x}TiO_3$ nanocubes synthesized by the composite-hydroxide-mediated approach. (A) XRD pattern of $BaTiO_3$ nanopowder. (B) SEM image of $BaTiO_3$ nanocubes; the inset is the EDS of the nanocubes showing the presence of Ba, Ti, and O. (C) TEM image of $BaTiO_3$ nanocubes; the insets are the electron diffraction pattern and HRTEM image of a nanocube, showing its single-crystal structure. (D) XRD pattern of $Ba_xSr_{1-x}TiO_3$ nanopowder. (E) TEM image of $Ba_xSr_{1-x}TiO_3$ nanopowder; the inset is the EDS of the nanocubes showing the presence of Ba, Sr, Ti, and O. The Cu signal came from the TEM grid. (F) A single-crystal $Ba_xSr_{1-x}TiO_3$ nanocube and its corresponding HRTEM image (inset).

A (A′) and B (B′) cations but also to lower the reaction temperature to ∼200°C or even less. A total of eight examples are selected here for illustrating this generalized approach.

Our first example is $BaTiO_3$, an important ferroelectric material.[1] The synthesis is performed in the following steps:[26] (i) An amount of 20 g of mixed hydroxides (NaOH/KOH = 51.5:48.5) (MHDs) was placed in a 25 mL Teflon vessel with a cover for preventing dust. (ii) A mixture of anhydrous $BaCl_2$ and TiO_2 at 0.5 mmol each was used as the raw material for reaction. (iii) The raw material was placed on the top of the hydroxide in the vessel. The vessel was put in a furnace, which was preheated to 200 °C. (iv) After the hydroxides were totally molten, the hydroxide solution was stirred by a platinum bar or by shaking the covered vessel to ensure the uniformity of the mixed reactants. (v) After reacting for 48 h, the vessel was taken out and cooled to room temperature. Deionized water was added to the solid product. The product was filtered and washed by first deionized water and then hot water to remove hydroxide on the surface of the particles. The synthesized product was received. For the next seven types of materials to be presented, all of the synthesis procedures are the same as those stated above except the raw materials in step ii are replaced.

X-ray diffraction (XRD) measurement proved that the as-synthesized product is tetragonal $BaTiO_3$ (*P*4*mm*, JCPD 81-2203) (Figure 1A). A scanning electron microscopy (SEM) image of the powder shows that the particles are 30−50 nm nanocubes or nanocuboids (Figure 1B), and energy-dispersive X-ray analysis (EDS) shows the presence of oxygen, barium, and titanium. Electron diffraction (ED) and high-resolution transmission electron microscope (HRTEM) images show that the nanocubes are single crystal and the three crystal faces are {100} planes (Figure 1C and inset).

From the above experimental results, a possible reaction mechanism for the synthesis of $BaTiO_3$ in hydroxide solution is suggested as follows. Although the melting points of both pure sodium hydroxide and potassium hydroxide are over 300 °C, T_m = 323 °C for NaOH and T_m = 360 °C for KOH, the eutectic point at NaOH/KOH = 51.5:48.5 is only about 165 °C. This is likely the key for synthesizing the complex oxide at ∼200 °C or lower. During the reaction process, hydroxides play a role not only as the solvent but also as the reactant for lowing the reaction temperature. In the molten hydroxide, TiO_2 reacts with NaOH/KOH and forms a hydroxide-soluble Na_2TiO_3/K_2TiO_3. To simplify the expression for chemical reactions here and after, we only include NaOH in the formula for simplicity:

$$2NaOH + TiO_2 \rightarrow Na_2TiO_3 + H_2O \quad (1)$$

At the same time, $BaCl_2$ reacts with hydroxide to form $Ba(OH)_2$, which is dissolved in the hydroxide solution:

$$BaCl_2 + 2NaOH \rightarrow Ba(OH)_2 + 2NaCl \quad (2)$$

The Na_2TiO_3 from process 1 reacts with the $Ba(OH)_2$ produced in process 2 and forms an indissoluble solid $BaTiO_3$:

$$Na_2TiO_3 + Ba(OH)_2 \rightarrow BaTiO_3 + 2NaOH \quad (3)$$

The Gibbs free energy following the above three steps for the formation of $BaTiO_3$ at 200 °C is calculated to be −24.16 kcal/mol.[27] Because the viscosity of hydroxide is large, the formation of $BaTiO_3$ nanostructure is slow and it is not easy

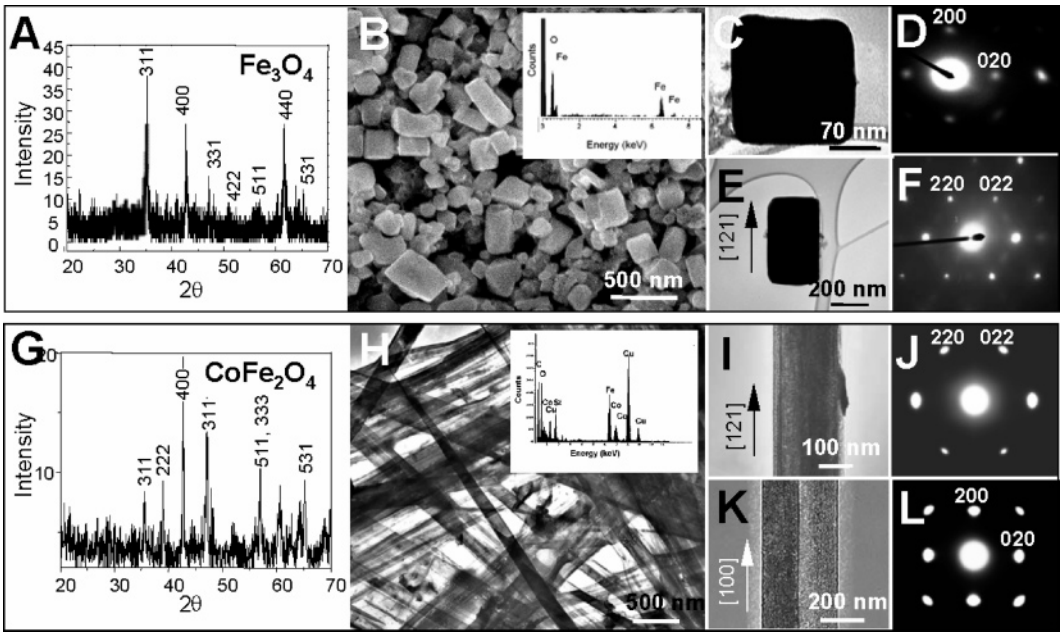

Figure 2. Synthesis of spinel nanostructures. (A−F) Fe_3O_4 nanoparticles and (G−L) $CoFe_2O_4$ nanobelts synthesized by the composite-hydroxide-mediated approach. (A) XRD pattern of Fe_3O_4. (B) SEM image of Fe_3O_4 nanoparticles and EDS pattern (inset). (C) A cubelike nanoparticle and (D) its electron diffraction pattern. (E) A Fe_3O_4 cuboid and (F) its diffraction pattern. (G) XRD pattern of $CoFe_2O_4$ nanobelts. (H) Morphology of the nanobelts and the corresponding EDS spectrum (inset) showing the presence of Co, Fe, and O. The Si signal came from the TEM grid and holder. (I) A single-crystal nanobelt growing along [121] and (J) its electron diffraction pattern. (K) A nanobelt growing along [100] and (L) its electron diffraction pattern.

for the nanostructures to agglomerate. This is likely the key for receiving dispersive single-crystalline nanostructures during the reaction without using an organic surface-capping material. The hydroxides mediate the reaction, but they are not part of the final nanostructures.

In the second example, $Ba_{0.5}Sr_{0.5}TiO_3$ was synthesized to explore the applicability of this method for synthesis of complex perovskites. Following the same procedures used for receiving $BaTiO_3$ except replacing the raw cation-supplying materials with a mixture of $BaCl_2$, $SrCl_2$, and TiO_2 at 0.5, 0.5, and 1.0 mmol, respectively. XRD pattern shows that the received product is a pure perovskite $Ba_{0.5}Sr_{0.5}TiO_3$ phase (Figure 1D). TEM measurement demonstrated that the powder product is nanocubes about 30−40 nm in size (Figure 1E). EDS measurement shows that the ratio of the elements in the product is Ba/Sr/Ti = 1:1:2, demonstrating the controllability in chemical composition. HRTEM observation proved that $Ba_{0.5}Sr_{0.5}TiO_3$ nanocubes are single crystals (Figure 1F and inset). However, there are some defects and atomic disorders in the crystal because strontium and barium share the same sites in the crystal, which possibly results in substitutional point defects. For both $BaTiO_3$ and $Ba_{0.5}Sr_{0.5}TiO_3$, the crystal face is clean and sharp, and no amorphous layer is present, because no organic reagent or capping material was introduced during the synthesis. The perovskite nanocubes with clean surfaces are desirable for investigating ferroelectricity at the nanoscale level and for building functional components.

A ferromagnetic spinel-structured complex oxide was chosen as the third example to demonstrate the extensive applicability of the synthesis method. To synthesize a spinel Fe_3O_4 ($Fe^{2+}Fe_2^{3+}O_4$) nanostructure, a mixture of anhydrous $FeCl_2$ and Fe_2O_3 at 0.5 mmol each was used as the raw material for providing Fe^{2+} and Fe^{3+} cations at the desired atomic ratio. The synthesis temperature and time were 200 °C and 72 h, respectively. XRD and EDS show that the product is cubic Fe_3O_4 (JCPDS 89-3854) (Figure 2A and inset in Figure 2B). In the product, most particles are nanocubes about 250 nm in size, and nanocuboids about 250 nm wide and 300−400 nm long. From ED patterns of single particles, we can see that the nanocubes and nanocuboids are single crystals. The faces of the nanocubes are the {100} crystallographic planes (Figure 2C and D). The growth direction of the nanocuboids is [121] (Figure 2E and F).

$CoFe_2O_4$ nanocrystals were synthesized as the fourth example. A mixture of $Co(NO_3)_2 \cdot 6H_2O$ and Fe_2O_3 at 0.5 mmol each was used as the raw material. XRD pattern demonstrated that the product is cubic $CoFe_2O_4$ (JCPDS 22-1086) (Figure 2G), as supported by EDS microanalysis (inset in Figure 2H). The morphology of $CoFe_2O_4$ is nanobelts about 20−40 nm thick, 150−250 wide, and more than 20 μm long (Figure 2H). ED shows that there are two kinds of belts growing along different directions, [121] and [100] (Figure 2I−L). The suggested formation mechanism of ferromagnetic MFe_2O_4 (M = Co, Fe, Ni, Co) spinel nanostructures is as follows:

$$MCl_2 + 2NaOH \rightarrow M(OH)_2 + 2NaCl;\ \text{or}\ M(NO_3)_2 + 2NaOH \rightarrow M(OH)_2 + 2NaNO_3 \quad (4)$$

$$Fe_2O_3 + NaOH \rightarrow Na_2Fe_2O_4 + H_2O \quad (5)$$

$$M(OH)_2 + Na_2Fe_2O_4 \rightarrow MFe_2O_4 + 2NaOH \quad (6)$$

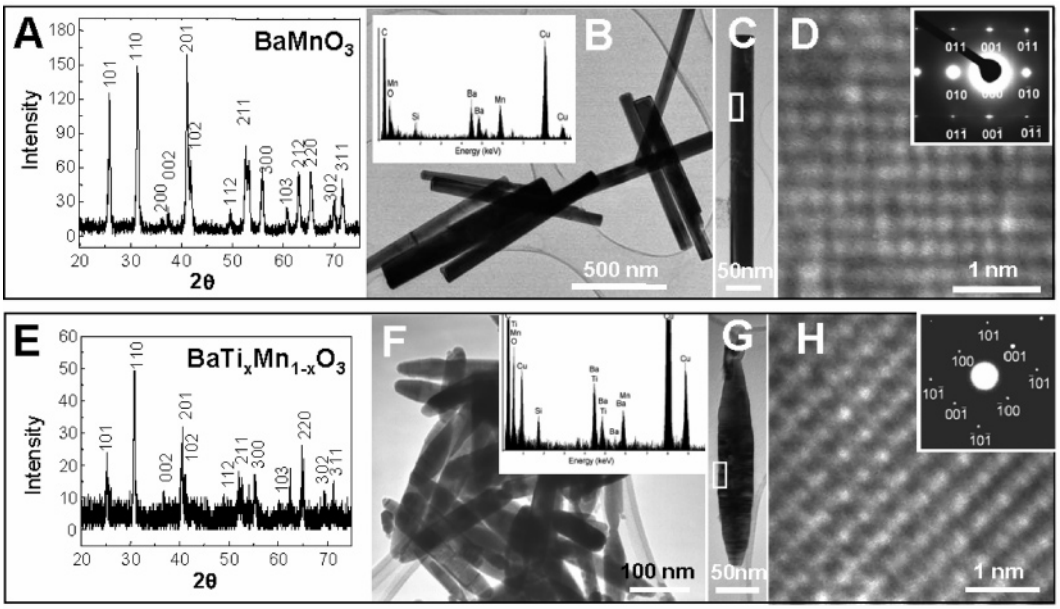

Figure 3. Synthesis of perovskite nanostructures. (A−D) $BaMnO_3$ and (E−H) $BaTi_{1-x}Mn_xO_3$ nanobelts synthesized by the composite-hydroxide-mediated approach. (A) XRD pattern of the $BaMnO_3$ nanobelts. (B) TEM image and EDS spectrum (inset) showing the presence of Ba, Mn, and O. The Si signal came from the TEM gird. (C) A single-crystal nanobelt and (D) its HRTEM image as well as corresponding electron diffraction pattern (inset) showing the [001] growth direction. (E) XRD pattern of $BaTi_xMn_{1-x}O_3$ nanopowder. (F) TEM image of the nanostructure. (G) A single-crystal nanostructure and (H) its HRTEM image as well as its electron diffraction pattern (inset).

To demonstrate the generality of the synthesis method, we chose colossal magnetoresistivity (CMR) materials,[2] such as $BaMnO_3$, as the fifth example. A mixture of $BaCl_2$ and MnO_2 was chosen as the cation supply material. The vessel was heated at 170 °C for 72 h during the synthesis. XRD pattern shows that the product is hexagonal $BaMnO_3$ (JCPDS-260168, $P6_3/mmc$) (Figure 3A), and EDS proved that there are only three types of elements, Ba, Mn, and O, in the sample (Figure 3B inset). The as-synthesized sample consists of nanobelts 20−30 nm thick, 50−80 nm wide, and 800−1000 nm long (Figure 3B). ED and HRTEM (Figure 3D and inset) show that the nanobelts are single crystals (Figure 3C). The flat surfaces are (100) plane, and the growth direction is [001]. The length and width of $BaMnO_3$ nanobelts can be adjusted by varying the reaction conditions, such as the heating temperature or/and heating time during the synthesis process.

When 50% of atoms at the Mn sites in barium manganite were substituted by Ti, $BaTi_{0.5}Mn_{0.5}O_3$ was received as the sixth example, which is a high-dielectric-constant material.[28] A mixture of $BaCl_2$, MnO_2, and TiO_2 at 0.422, 0.221, and 0.221 mmol, respectively, was used as the raw material for the synthesis. XRD measurement shows that the crystalline structure of the material is the same as that of $BaMnO_3$ (Figure 3E), and EDS shows that the atomic ratio of Ba/Ti/Mn is about 1:0.5:0.5 (inset of Figure 3F). The morphology of $BaTi_{0.5}Mn_{0.5}O_3$ is different from that of $BaMnO_3$ and $BaTiO_3$ (Figure 3F). The particles are elliptical nanobelts about 40 nm wide, 20 nm thick, and 500 nm long. ED and HRTEM show that each nanobelt is a single crystal (Figure 3G) with a flat plane of (010). The growth direction is [101]. The formation of $Ba(Ti_xMn_{1-x})O_3$ is described by eqs 10−11. The mechanism about the formation of $BaMnO_3$ is described as follows:

$$BaCl_2 + NaOH \rightarrow Ba(OH)_2 + 2NaCl \quad (7)$$

$$MnO_2 + 2NaOH \rightarrow Na_2MnO_3 + H_2O \quad (8)$$

and

$$Ba(OH)_2 + Na_2MnO_3 \rightarrow BaMnO_3 + 2NaOH \quad (9)$$

For $Ba(Ti_xMn_{1-x})O_3$:

$$xTiO_2 + (1-x)MnO_2 + 2NaOH \rightarrow Na_2(Ti_xMn_{1-x})O_3 + H_2O \quad (10)$$

and

$$Ba(OH)_2 + Na_2(Ti_xMn_{1-x})O_3 \rightarrow Ba(Ti_xMn_{1-x})O_3 + 2NaOH \quad (11)$$

The seventh example is perovskite $BaCeO_3$ containing a rare earth metal element, which is a new material that has applications as hydrogen sensors, fuel cells, phosphor, and electrolyzers.[29] A mixture of anhydrous $BaCl_2$ and CeO_2 at 0.5 mmol each was used as the raw material for the synthesis. XRD shows that the product is a tetragonal perovskite (JCPDS-35-1318) structure (Figure 4A). A SEM image shows that the product is a flowerlike nanostructure. The thickness of the leaflike structure is 20−30 nm, the maximum

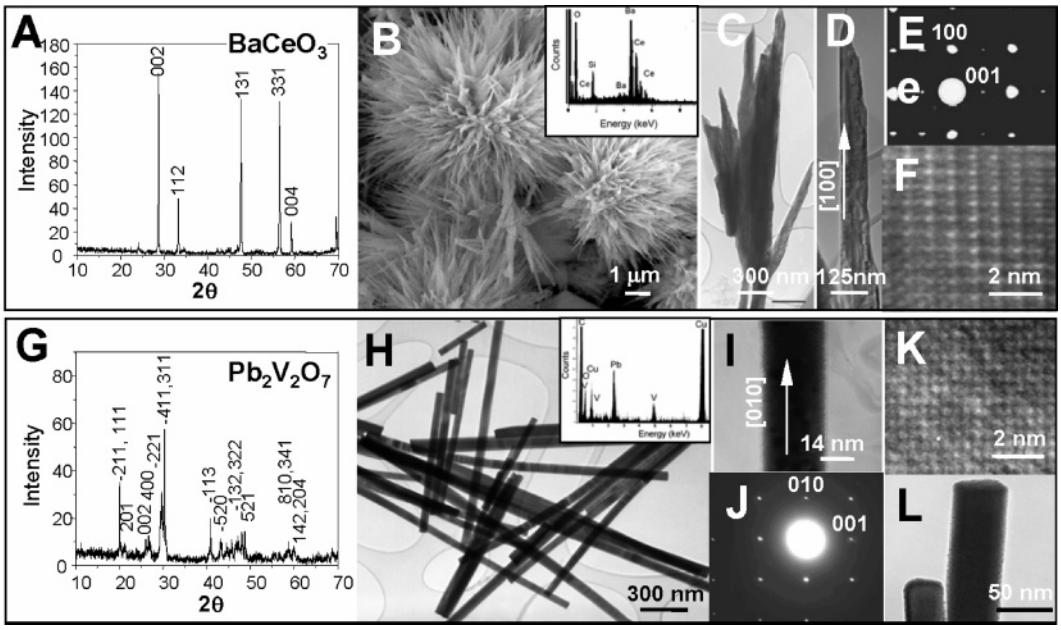

Figure 4. Synthesis nanostructures of rare earth-metal-dominated oxides. (A−F) $BaCeO_3$ nanoflowers and (G−L) $Pb_2V_2O_7$ nanobelts synthesized by the composite-hydroxide-mediated approach. (A) XRD pattern of $BaCeO_3$ nanoflowers. (B) Morphology of the nanoflowers and the EDS spectrum (inset) showing the presence of Ba, Ce, and O. The Si signal came from the Si substrate. (C) A branch of the nanoflower. (D) A single-crystal leaf of the nanoflower and its (E) electron diffraction pattern and (F) corresponding HRTEM image. (G) XRD pattern of $Pb_2V_2O_7$ nanoparticles. (H) Morphology of $Pb_2V_2O_7$ nanobelts. (I) A single-crystal nanobelt and its (J) electron diffraction pattern, as well as (K) its corresponding HRTEM image. (L) Rectangular cross section of a nanobelt.

width is 150−180 nm, and the length is up to micrometers (Figure 4B). Elemental analysis by EDS supports the XRD result (inset of Figure 4B). Figure 4C and E shows the typical shapes of the leaves. From the ED pattern and HRTEM image of the leaf, each leaf is a single crystal. The large surface of the leaf is (010), and its growth direction is [100]. The formation mechanism of $BaCeO_3$ is similar to that for $BaTiO_3$ and $BaMnO_3$.

As the last example, Pb−V−O was chosen to demonstrate the approach for even more complex structure types other than the perovskite and spinel families. Pb−V−O complexes have low resistivity and novel magnetic properties.[30,31] A mixture of V_2O_5 and anhydrous $Pb(NO_3)_2$ at 0.5 mmol each was used as the raw material for the synthesis. The crystalline phase and the ration of elements of the product was proved to be monoclinic $Pb_2V_2O_7$ (JCPDS 70-1547, $P2_1/c$) by XRD (Figure 4G) and EDS (inset of Figure 4H). The nanostructure has the morphology of nanobelts with widths of 50−70 nm, thicknesses of 25−30 nm, and lengths of several micrometers (Figure 4H). The diffraction pattern (Figure 4J) and HRTEM image (Figure 4K) from a nanobelt (Figure 4I) show its single-crystal structure with a (100) flat surface and [010] growth direction. Figure 4L shows that the cross section of the nanobelt is rectangular. The suggested mechanism about the formation of $Pb_2V_2O_7$ is as follows:

$$Pb(NO_3)_2 + 2NaOH \rightarrow Pb(OH)_2 + 2NaNO_3 \quad (12)$$

$$V_2O_5 + 4NaOH \rightarrow Na_4V_2O_7 + 2H_2O \quad (13)$$

$$2Pb(OH)_2 + Na_4V_2O_7 \rightarrow Pb_2V_2O_7 + 4NaOH \quad (14)$$

In summary, this paper demonstrates a generic approach for synthesis of complex oxide nanostructures of various structure types. Examples have been presented for representing perovskites ($BaTiO_3$, $Ba_{0.5}Sr_{0.5}TiO_3$, $BaMnO_3$, $BaTi_{0.5}Mn_{0.5}O_3$, $BaCeO_3$), spinels (Fe_3O_4, $CoFe_2O_4$), monoclinic ($Pb_2V_2O_7$), and more. The received nanostructures of the complex oxides exhibit properties in ferroelectricity, ferromagnetism, colossal magnetoresistance, fuel cell, optics, and more. The synthesis technique has the following unique advantages. First, it is a simple, one-step, and slow-reaction synthesis approach, making it easy to control growth kinetics for tuning the size and morphology of the synthesized nanostructure. Second, the synthesis is at lower growth temperature of ∼200 °C at normal atmosphere in an open container, and it needs no expensive or sophisticated equipment; thus, the technique can be easily adopted and transferred for technological applications. Third, the raw materials are cheap and the entire synthesis process is cost-effective. The yield is high and it is readily expandable for large-scale production to meet the needs of industry. Fourth, all of the as-received nanostructures are high-quality single crystals, which are required for many applications. Fifth, there is neither a capping reagent nor an amorphous layer on the surfaces of the as-synthesized nanostructures; thus, the clean surfaces can be readily functionalized for various applications. Finally, the synthesis process is nontoxic without producing hazardous waste. The technique can be expanded to many material systems, and it provides a general, simple, convenient, and innovative strategy for the synthesis of nanostructures of complex oxides with important scientific and technological applications.

Acknowledgment. Thanks to support from NSF (DMR 9733160), CCNE from NIH, NSFC (50572052, 60376032), the NASA Vehicle Systems Program and Department of Defense Research and Engineering (DDR&E), Fellowships from Chongqing University (C.G.H.), and the Chinese Minister of Education (H.L.).

Supporting Information Available: Experimental principle and additional data for demonstrating the synthesis technique. This material is available free of charge via the Internet at http://pubs.acs.org.

References

(1) Cohen, R. E. *Nature* **1992**, *358*, 136−138.
(2) Moritomo, Y.; Asamitua, A.; Kuwahara, H.; Tokura, Y. *Nature* **1996**, *380*, 141−144.
(3) Lacorre, P.; Goutenoire, F.; Bohnke, O.; Retoux, R.; Laligant, Y. *Nature* **2000**, *404*, 856−858.
(4) Anderson, P. W.; Abrahams, E. *Nature* **1987**, *327*, 363−363.
(5) Tarascon, J.-M.; Armand, M. *Nature* **2001**, *414*, 359−367.
(6) Homes, C. C.; Vogt, T.; Shapiro, S. M.; Wakimoto, S.; Ramirez, A. P. *Science* **2001**, *293*, 673−676.
(7) Pan, Z. W.; Dai, Z. R.; Wang, Z. L. *Science* **2001**, *291*, 1947−49.
(8) Yin, Y.; Rioux, R. M.; Erdonmez, C. K.; Hughes, S.; Somorjai, G. A.; Alivisatos, A. P. *Science* **2004**, *304*, 711−714.
(9) Ryan, J. V.; Berry, A. D.; Anderson, M. L.; Long, J. W.; Stroud, R. M.; Cepak, V. M.; Browning, V. M.; Rolison, D. R.; Merzbacher, C. I. *Nature* **2000**, *406*, 169−172.
(10) Yin, Y.; Alivisatos, A. P. *Nature* **2005**, *437*, 664−670.
(11) Redl, F. X.; Cho, K. S.; Murray, C. B.; O'Brien, S. *Nature* **2003**, *423*, 968−971.
(12) Park, J.; An, K.; Hwang, Y.; Park, J.-G.; Noh, H.-J.; Kim, J.-Y.; Park, J.-H.; Hwang, N.-M.; Hyeon, T. *Nat. Mater.* **2004**, *3*, 891−895.
(13) Zhou, Y.; Schattka, J.; Antonietti, M. *Nano Lett.* **2004**, *4*, 477−431.
(14) Yang, L.; Zhu, Y.; Wang, Y.; Tong, H.; Ruan, M. *J. Phys. Chem. B* **2006**, *110*, 6609−6614.
(15) Wang, X.; Zhuang, J.; Peng, Q.; Li, Y. *Nature* **2005**, *437*, 121−124.
(16) Brien, S. O.; Brus, L.; Murray, C. B. *J. Am. Chem. Soc.* **2001**, *123*, 12085−12086.
(17) Urban, J. J.; Yun, W. S.; Gu, Q.; Park, H. *J. Am. Chem. Soc.* **2002**, *124*, 1186−1187.
(18) Mao, Y.; Banerjee, S.; Wong, S. S. *J. Am. Chem. Soc.* **2003**, *125*, 15718−15719.
(19) Urban, J. J.; Ouyang, L.; Jo, M.; Wang, D. S.; Park, H. *Nano Lett.* **2004**, *4*, 47−49.
(20) Xu, G.; Ren, Z.; Du, P.; Weng, W.; Shen, G.; Han, G. *Adv. Mater.* **2005**, *17*, 907−910.
(21) Niederberger, M.; Pinna, N.; Polleux, J.; Antonietti, M. *Angew. Chem., Int. Ed.* **2004**, *43*, 2270−2273.
(22) Song, Q.; Zhang, Z. *J. Am. Chem. Soc.* **2004**, *126*, 6164−6168.
(23) Sun, S.; Zeng, H.; Robinson, D. B.; Raoux, S.; Rice, P. M.; Wang, S. X.; Li, G. *J. Am. Chem. Soc.* **2004**, *126*, 273−279.
(24) Hyeon, T.; Chung, Y.; Park, J.; Lee, S. S.; Kim, Y.-W.; Park, B. H. *J. Phys. Chem. B* **2002**, *106*, 6831−6833.
(25) Wang, Z. L.;Kang, Z. C. *Functional and Smart Materials*; Plenum Press: New York, 1998; Chapter 3.
(26) The experimental procedures are protected by an U.S. provisional patent.
(27) Dean, J. A. *Lange's Handbook of Chemistry*, 15th ed.; McGraw-Hill: New York, 1999.
(28) Keith, G. M.; Kirk, C. A.; Sarma, K.; Alford, N. McN.; Cussen, E. J.; Rosseinsky, M. J.; Sinclair, D. C. *Chem. Mater.* **2004**, *16*, 2007−2015.
(29) Pena, M. A.; Fierro, J. L. G. *Chem. Rev.* **2001**, *101*, 1981−2017.
(30) Shpachenko, R. V.; Chernaya, V. V.; Abakumov, A. M.; Antipov, E. V.; Hadermann, J.; Van Tendeloo, G.; Kaul, E. E.; Geibel, C.; Sheptyakov, D.; Balagurov, A. M. *Z. Anorg. Allg. Chem.* **2001**, *627*, 2143−2150.
(31) Mentre, O.; Dhaussy, A. C.; Abraham, F. *Chem. Mater.* **1999**, *11*, 1, 2408−2416.

NL061253E